The influence of continental ice, atmospheric CO_2, and land albedo on the climate of the last glacial maximum

A J Broccoli and S Manabe

Geophysical Fluid Dynamics Laboratory/NOAA, Princeton University, P.O. Box 308, Princeton, NJ 08542, USA

Abstract. The contributions of expanded continental ice, reduced atmospheric CO_2, and changes in land albedo to the maintenance of the climate of the last glacial maximum (LGM) are examined. A series of experiments is performed using an atmosphere-mixed layer ocean model in which these changes in boundary conditions are incorporated either singly or in combination. The model used has been shown to produce a reasonably realistic simulation of the reduced temperature of the LGM (Manabe and Broccoli 1985b). By comparing the results from pairs of experiments, the effects of each of these environmental changes can be determined.

Expanded continental ice and reduced atmospheric CO_2 are found to have a substantial impact on global mean temperature. The ice sheet effect is confined almost exclusively to the Northern Hemisphere, while lowered CO_2 cools both hemispheres. Changes in land albedo over ice-free areas have only a minor thermal effect on a global basis. The reduction of CO_2 content in the atmosphere is the primary contributor to the cooling of the Southern Hemisphere. The model sensitivity to both the ice sheet and CO_2 effects is characterized by a high latitude amplification and a late autumn and early winter maximum.

Substantial changes in Northern Hemisphere tropospheric circulation are found in response to LGM boundary conditions during winter. An amplified flow pattern and enhanced westerlies occur in the vicinity of the North American and Eurasian ice sheets. These alterations of the tropospheric circulation are primarily the result of the ice sheet effect, with reduced CO_2 contributing only a slight amplification of the ice sheet-induced pattern.

1. Introduction

During the past decade, a more complete picture has emerged of the ice age earth and its atmoshpere. A major

Offprint requests to: AJ Broccoli

contribution to this improved understanding of conditions during a glacial period was made by the CLIMAP Project (CLIMAP Project Members, 1976, 1981), which reconstructed characteristics of the earth's surface for the time of the last glacial maximum (approximately 18 000 years B.P.). CLIMAP used a variety of geological evidence to reconstruct the reduced sea level of glacial time, the extent and elevation of continental ice sheets, and the distributions of sea surface temperature (SST), sea ice, and surface albedo. The CLIMAP reconstructions represented the first quantitative estimates of ice age surface characteristics on a global basis.

In addition, chemical analyses of air bubbles trapped in ice cores from the Greenland and Antarctic ice sheets have made possible estimates of the atmospheric composition during the last glacial maximum. Neftel et al. (1982) have estimated that the atmospheric CO_2 concentration at 18 000 years B.P. was between 200 and 230 ppm, as compared to the present day concentration of 340 ppm. Using a different method, Shackleton et al. (1983) found confirming evidence of reduced atmospheric CO_2 during the last glacial period by analyzing the carbon-13 content of marine microfossils.

Progress has also occurred in understanding the causes of the glacial-interglacial fluctuations in climate during the Pleistocene. Hays et al. (1976) demonstrated the relationship between variations in the earth's orbital parameters and fluctuations of global climate using evidence from deep-sea cores. Their work provided quantitative support for the hypothesis offered by Milankovitch (1941) that changes in the seasonal distribution of solar radiation resulting from the varying orbital parameters were the cause of the ice ages.

The compilation of this information about the ice age earth has stimulated a number of studies in which atmospheric general circulation models (GCMs) have been used in attempts to simulate the climate of the last glacial maximum (LGM). Such studies are made possible by the availability of some or all of the information described

previously for use as input (i. e., boundary conditions) to the GCMs. Gates (1976a, b), Manabe and Hahn (1977), and Hansen et al. (1984) simulated the ice age climate using the CLIMAP reconstructions in this way. In each of these studies, the distributions of SST, sea ice, surface albedo, and continental ice were prescribed as surface boundary conditions for the models.

A somewhat different approach was taken by Manabe and Broccoli (1985a) in a study of the effects of continental ice sheets on climate. They used an atmospheric GCM coupled with a simple model of the oceanic mixed layer. In their climate model, it was necessary to specify land surface conditions only, since SST and sea ice were predicted by the oceanic model. This allowed the CLIMAP estimates of SST and sea ice to be used as a standard to which the response of the model was compared.

In a model validation study, Manabe and Broccoli (1985b) used two versions of a similar model (with and without interactive cloud cover) to simulate the climate of the LGM. The CLIMAP distributions of continental ice and land surface albedo were used as model input along with a reduced atmospheric CO_2 concentration. A comparison of the LGM climates simulated by the models with the CLIMAP SSTs and land-based paleoclimatic data indicated a general agreement despite some significant discrepancies in low latitudes. This suggests that the models may be used with more confidence in studies of ice age climate.

In the present study, the contributions of continental ice, reduced CO_2, and changes in surface albedo over ice-free areas to the maintenance of the LGM climate are examined. The contribution of changes in orbital parameters is not studied, since at the time of the LGM they were very similar to their present values. The fixed cloud version of the atmosphere-mixed layer ocean model of Manabe and Broccoli (1985b) is used, thus the effects of cloud feedback are not included. While Manabe and Broccoli found that the incorporation of interactive cloudiness produced an increase in model sensitivity in simulating the LGM climate, the fixed cloud version is preferred because of its simplicity of analysis.

Given the overall success of this model in simulating the LGM climate, this study is a natural extension of the previous work. A series of climate model experiments is run, with each experiment incorporating the LGM changes in boundary conditions singly or in combination. The response of the model to a particular change in boundary conditions is determined by comparing runs with and without that change. This study primarily examines the changes in radiative forcing, temperature and atmospheric circulation brought on by the changes in boundary conditions. This strategy should allow some insight to be gained about how these factors combine to produce the cold ice age climate.

2. Model structure and experimental design

The climate model used for this study is constructed by coupling a global atmospheric GCM with a simple model of the oceanic mixed layer. The atmospheric GCM uses the so-called semi-spectral method, in which the horizontal distributions of atmoshperic variables are represented by spherical harmonics and gridpoint values (Gordon and Stern 1982; Bourke 1974). The model's horizontal resolution is determined by the degree of truncation of the spectral components. For the model used in this study, 15 zonal waves have been retained, adopting the so-called rhomboidal truncation. The grid spacing is chosen to be 4.5 ° latitude by 7.5 ° longitude. The oceanic mixed layer model consists of a static, isothermal layer of water with uniform thickness. The process of sea ice formation is explicitly incorporated into the model, but the effects of heat transport by ocean currents are not included. Seasonally-varying insolation is prescribed at the top of the atmosphere, but diurnal variation is not included. Zonally uniform cloud cover is prescribed with respect to latitude and height but does not vary with season.

This model is identical to the fixed cloud model used by Manabe and Broccoli (1985b), and is essentially the same as the model described by Manabe and Stouffer (1980) with the following exceptions: (1) the meridional distribution of total cloud cover is taken from Berlyand et al. (1980) and the vertical distribution from London (1957); (2) the thickness of the oceanic mixed layer is set at 50 m to yield a realistic amplitude of the seasonal cycle of SST; and (3) the albedo values assigned to snow and sea ice are slightly modified as specified below.

The albedo of snow cover depends on latitude and snow depth. For deep snow (water equivalent at least 1 cm), the surface albedo is 60% equatorward of 55 °, 80% poleward of 66.5 °, with a linear interpolation between these values from 50 ° to 66.5 °. When the water equivalent of the snow depth is less than 1 cm, it is assumed that the albedo decreases from the deep snow values to the albedo of the underlying surface as a square root function of snow depth. In an analogous manner, the albedo of sea ice depends on latitude and ice thickness. For thick sea ice (at least 0.5 m thick), the surface albedo is 50% equatorward of 50 °, 80% poleward of 70 °, with a linear interpolation between these values from 50 ° to 70 °. The formation of meltwater puddles is parameterized by lowering the surface albedo by 20% from the thick sea ice values when the ice is melting. If the ice thickness is less than 0.5 m, the albedo is further reduced to the lower albedo of the underlying water surface as a square root function of ice thickness.

The performance of this model in simulating the present climate is reasonably good. Surface air temperatures simulated by the model are quite close to observed values throughout the Northern Hemisphere and much of the Southern Hemisphere. South of 45S the model is somewhat
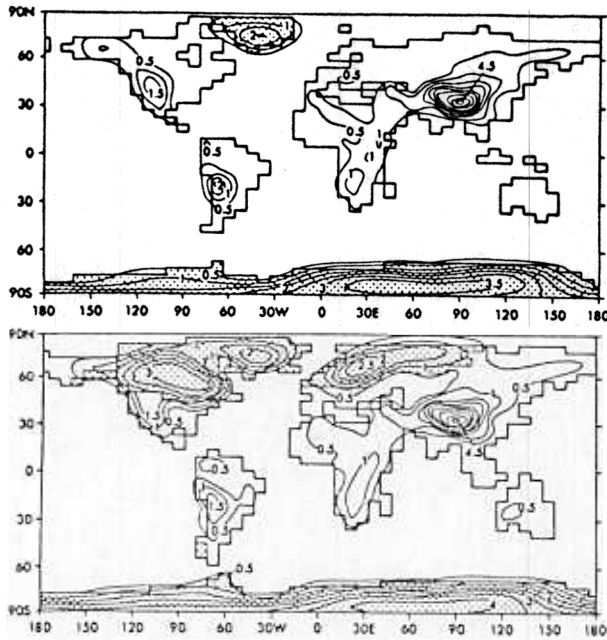
Fig. 1. Continental outlines, topography, and distribution of continental ice used in model experiments. Topographic contours indicate height above sea level (km). Regions covered by continental ice are stippled. *Top*: present. *Bottom*: last glacial maximum

Table 1. Boundary conditions and length of analysis period for atmosphere-mixed layer ocean model experiments (*P*: present, *L*: last glacial maximum)

Experiment	E1	E2	E3	E4
Land-Sea Distribution	P	L	L	L
Continental Ice Distribution	P	L	L	L
Atmospheric CO_2 Concentration (ppm)	300	300	300	200
Snow-Free Land Albedo Distribution	P	P	L	L
Length of Analysis Period (years)	15	8	6	8

too warm, especially over Antarctica. This represents an improvement over the simulation of Manabe and Stouffer (1980), where the Southern Hemisphere warm bias was larger and more widespread. The changes in the prescribed cloud cover are primarily responsible for the marked reduction of this bias. Manabe and Broccoli (1985b) discuss this model's performance in simulating the present and LGM climates in more detail.

Using this model, a series of four experiments was run, each incorporating a different set of boundary conditions. The boundary conditions used in each experiment are listed in Table 1. The present and LGM coastlines and distributions of continental ice and topography are pictured
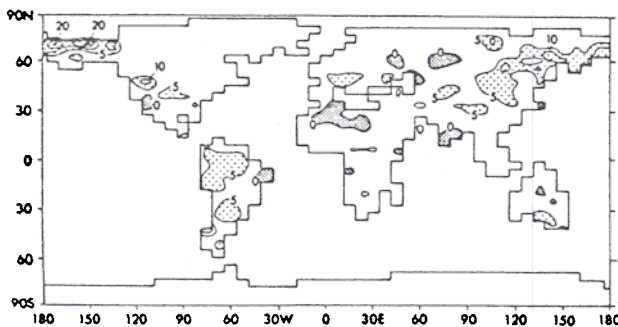

Fig. 2. Difference in base albedo (i. e., surface albedo in the absence of snow cover) of land areas (%) between the LGM and the present. *Dense stippling* indicates a decrease in albedo, and *light stippling* an increase in albedo larger than 5%

in Fig. 1, and the differences in bare land albedo between the LGM and the present are shown in Fig. 2.

In each experiment, a substantial period of integration (~30–40 years) was required in order for a quasi-equilibrium model climate to be established. The models were then integrated for an additional period, ranging from 6 to 15 years, to provide an adequate sample for analysis. The exact length of the analysis period for each experiment is included in Table 1. Each of the experiments with the exception of E3 was started from an initial state consisting of a dry, isothermal atmosphere at rest coupled to an isothermal mixed layer ocean. A sample from the quasi-equilibrium period of E2 was used as the initial state for E3 in an effort to save computer time. [E1 and E4 are the standard simulation and LGM simulation used in the study by Manabe and Broccoli (1985b).] By making comparisons between pairs of experiments, the response of the model to changes in continental ice, atmospheric CO_2, and land albedo will be examined.

3. Radiative forcing

Each of the changes in boundary conditions being studied has a direct impact on the radiation budget of the model. Due to the high albedo of ice and snow, changes in the distribution of continental ice affect the net incoming solar radiation. Changes in land albedo also have a similar effect. The reduction of atmospheric CO_2 content exerts an important influence on radiative transfer, primarily in the longwave portion of the spectrum. Before discussing the results of the experiments described in the previous section, the magnitude of the radiative forcing associated with each of these changes is examined.

The direct effects of these changes on the model's radiation budget cannot be evaluated from the experiments described in the previous section, since these effects are modified by a number of climatic feedbacks that are present in the model. In order to determine the magnitude of the direct radiative forcing associated with each of the changes in boundary conditions, it is necessary to perform a pair of radiation-only calculations using the model's radiative transfer algorithm. A control calculation determines the net radiative flux at the top of the atmosphere. Then, in a

Table 2. Radiative forcing calculations performed for each change in boundary conditions. $\Delta R = \Delta S - \Delta F$, where ΔS is the change in annual mean net incoming solar radiation and ΔF is the change in annual mean net outgoing longwave radiation. Values are in $W\,m^{-2}$

Control Experiment	Perturbation	ΔR		
		Global	N. Hem.	S. Hem.
E1	LGM distribution of continental ice	-0.88	-1.71	-0.06
E3	atmospheric CO_2 reduced to 200 ppm	-1.28	-1.24	-1.31
E2	LGM distribution of land albedo	-0.67	-0.77	-0.58

perturbation calculation, the change in this flux resulting from a particular effect can be evaluated with all other factors kept constant.

For example, to examine the radiative forcing associated with the expanded continental ice sheets, the simulation of the present climate (E1) is used for the control. Changes in the base albedo (i. e., the surface albedo in the absence of snow cover) of gridpoints covered by continental ice during the LGM but not at present constitute the perturbation. (It should be noted that the ice sheet-induced radiative forcing calculated in this fashion does not include the effect of the elevated ice surface on longwave radiation.) Estimation of the land albedo effect is accomplished in much the same way, with changes in base albedo resulting from differences in vegetation and soil type as the perturbation. These changes may not affect the radiative flux at all locations, since they may be masked by snow cover. In the case of reduced CO_2, lowering the atmospheric CO_2 content constitutes the perturbation.

The results from these radiative calculations are expressed as changes in the net incoming radiation at the top of the atmosphere and are presented in Table 2. The annual mean forcing was estimated by averaging the results of calculations for the months of January, April, July, and October. On a global basis, the radiative forcing associated with the reduced CO_2 of the LGM is the largest of the three, followed by the ice sheet and land albedo effects. The magnitude of the radiative forcing produced by lowered CO_2 is similar in each hemisphere, as is the case with the land albedo effect. In contrast, the radiative forcing associated with changes in the ice sheet distribution occurs almost exclusively in the Northern Hemisphere. This is reasonable, since the expanded continental ice that characterized the LGM was found primarily in the Northern Hemisphere.

4. Response of sea surface temperature

One of the most prominent climatic effects produced by the inclusion of LGM boundary conditions in the model is the cooling of both the atmosphere and mixed layer ocean. In this section, the changes in SST associated with incorporating each of the changes in boundary conditions will be examined. The choice of SST as the first climatic parameter to be discussed is motivated by the availability of the CLIMAP estimates of the LGM SST distribution for comparison with the model results. Changes in atmospheric temperature will be discussed in a subsequent section.

The individual effects of each change in boundary conditions can be examined by making comparisons between experiments. The effects of expanded continental ice can be evaluated by comparing experiments E2 and E1. Similarly, differences between the simulated climates of experiments E4 and E3 represent the effects of reduced CO_2, while a comparison of experiments E3 and E2 yields the effects of changes in land albedo.

As a measure of the large-scale cooling that occurs in the model, the annual mean reduction of area-averaged SST associated with each of the changes in boundary conditions is presented in Table 3. The simulated LGM reduction of SST (produced by including all of the changes in boundary conditions) and the SST reduction estimated by CLIMAP are also included. A comparison of the simulated and CLIMAP values reveals that while the SST cooling produced by the model is slightly larger, it is quite similar to the CLIMAP estimates. The model simulates a reduction in SST in the Northern Hemisphere that is larger than that in the Southern Hemisphere, a finding which is consistent with the CLIMAP estimates. A more detailed analysis of SST changes in the LGM simulation can be found in Manabe and Broccoli (1985b).

In comparing the individual effects of each of the changes in boundary conditions to their combined effect, it is found that the sum of the ice sheet, CO_2, and albedo effects is approximately equal to the combined effect. On a global basis, the CO_2 effect produces just over half of the 1.9 °C simulated LGM cooling, while the ice sheet effect contributes somewhat less than half. The effect of the changes in surface albedo is small, producing only a 0.2 °C cooling. The partitioning of the response between the Northern and Southern Hemispheres varies considerably.

Table 3. Differences in area-averaged annual mean SST between pairs of experiments (°C). CLIMAP estimates of SST differences between the LGM and the present are also included for comparison. Only those gridpoints that represent oceans in all experiments are used in computing these values

		Global	N. Hem.	S. Hem.
E2-E1	(Ice Sheet)	-0.8	-1.6	-0.2
E4-E3	(CO_2)	-1.0	-0.7	-1.1
E3-E2	(Albedo)	-0.2	-0.3	-0.2
E4-E1	(Combined)	-1.9	-2.6	-1.5
CLIMAP		-1.6	-1.9	-1.3

Changes in surface albedo produce a reduction in SST that is approximately equal in both hemispheres. This is not the case for the effects of continental ice, which produces a very large Northern Hemisphere response and only a slight Southern Hemisphere cooling. The hemispheric asymmetry is less pronounced for the effects of reduced CO_2 on SST, which are about 50% larger in the Southern Hemisphere.

This emphasizes the difference in importance of each change in boundary conditions to the SST reduction in each hemisphere. For the Northern Hemisphere, just over 60% of the ice age cooling is associated with the increased extent of continental ice, making it by far the most important contributor. Reduced atmospheric CO_2 and the vegetation-induced changes in surface albedo make substantially smaller contributions to the model's LGM cooling. In contrast, the lowered CO_2 content of the atmosphere alone accounts for more than 70% of the Southern Hemisphere ice age cooling, with the changes in continental ice and surface albedo contributing almost equally to the remainder. This is consistent with the results of Manabe and Broccoli (1985a), who found little Southern Hemisphere cooling as a result of introducing the LGM distribution of continental ice into a similar climate model.

The latitudinal profiles of the SST response to each of the changes in boundary conditions is presented in Fig. 3. Four curves are plotted, each representing the annual mean difference in zonal mean SST from the following pairs of experiments: E2-E1, E4-E3, E3-E2, and E4-E1. These represent the changes in SST in response to the ice sheet, CO_2, and albedo effects, and in response to all three effects combined. The SST differences between the LGM and the present as reconstructed by CLIMAP are also plotted for comparison with those simulated by the model. This comparison reveals that the LGM simulation (E4-E1) is quite good in the middle latitudes of the Northern Hemisphere, near the equator, and in the Southern Hemisphere south of 30S. Elsewhere, the model over-

estimates the magnitude of the LGM cooling in the subtropics of both hemispheres and underestimates it in the high latitude Northern Hemisphere. A more complete discussion of this comparison appears in Manabe and Broccoli (1985b).

In examining the individual responses to each change in boundary conditions, the extreme asymmetry of the response to expanded continental ice is again evident. Maximum cooling occurs between 50–60N, with the response diminishing rapidly equatorward to become quite small south of the equator. A weak maximum appears at about 60S indicating the influence of the expanded Antarctic ice sheet. Reduced CO_2 produces a more symmetric response, although larger in the Southern Hemisphere. It is also responsible for a relatively uniform cooling of between 0.5 and 1.0 °C throughout the tropics, the major contribution to tropical SST reduction in the model. Changes in surface albedo cause SST to decrease by only a relatively small amount in all latitudes, with the largest response between 0–40N, where land surface albedos during the LGM were higher than their present values over large areas.

The absence of high latitude cooling of SST in response to the ice sheet and CO_2 effects requires further explanation. Since SST represents the temperature of the model's mixed layer ocean, it has a value of −2 °C (i. e., the freezing point of sea water) in areas covered by sea ice. For this reason, no reduction in SST is possible at grid points that are already ice-covered, and the potential for SST reduction is limited at those points where the SST is close to freezing. Thus the location of the maximum reduction in SST bears a close association with the location of the LGM sea ice margin, and the reduction of SST poleward of that margin is limited. Manabe and Broccoli (1985a) describe this phenomenon in more detail.

5. Response of surface air temperature

Although some measure of the thermal impact of incorporating each of the changes in boundary conditions can be derived by examining the resulting changes in SST, it is more useful to study the climatic effects in continental as well as oceanic locations. Surface air temperature, defined as the temperature at the model's lowest finite-difference level ($\sim$ 80 m above the surface), is indicative of near-
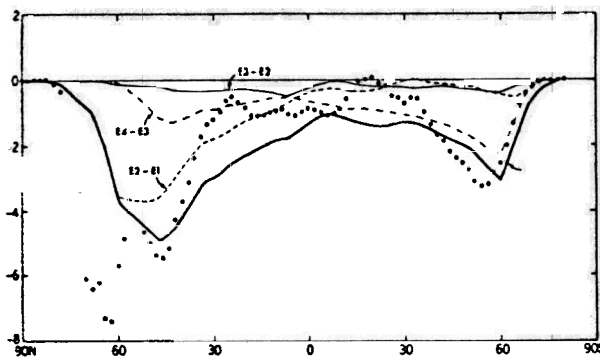

Fig. 3. Latitudinal distribution of annually averaged difference in zonal mean sea surface temperature (°C). Only gridpoints that represent oceans in all four experiments are used in computing the differences. The *solid circles* indicate the differences in sea surface temperature between the last glacial maximum and present as reconstructed by CLIMAP

Table 4. Differences in area-averaged annual mean surface air temperature (°C) between pairs of experiments. Only gridpoints free of continental ice in all four experiments are used in computing the differences

		Global	N. Hem.	S. Hem.
E2-E1	(Ice sheet)	−1.3	−2.4	−0.3
E4-E3	(CO_2)	−1.2	−1.1	−1.3
E3-E2	(Albedo)	−0.3	−0.4	−0.3
E4-E1	(Combined)	−2.8	−3.9	−1.9

surface thermal conditions over both land and sea. Table 4 contains differences in annual mean surface air temperature computed from each of the pairs of experiments discussed previously. In computing these temperature differences, only gridpoints free of continental ice in all four experiments are used. At all other gridpoints the surface elevation varies among the four experiments due to the changes in the extent and thickness of continental ice. Using only the ice-free gridpoints eliminates the trivial effect of surface elevation on temperature, which is not indicative of large scale climate change.

These differences indicate that the expanded continental ice produces the largest contribution to the reduction of surface air temperature, with reduced CO_2 a very close second. This contrasts with the analysis of changes in global mean SST, in which the effect of reduced CO_2 is somewhat larger. In all other respects, the relative effects of incorporating each of the changes in boundary conditions are similar for surface air temperature and SST. In the Northern Hemisphere, the ice sheet effect is most important, while in the Southern Hemisphere reduced CO_2 has the largest effect. Changes in surface albedo are relatively unimportant in both hemispheres.

When the radiative forcing associated with each of the LGM changes in boundary conditions is compared with the changes in surface air temperature described above, it is evident that the thermal response is not proportional to the forcing. Both the response to expanded continental ice and to reduced CO_2 are larger relative to the forcing than the response to changes in land albedo. To understand this contrast, it is necessary to consider the geographical distribution of the radiative forcing and its impact on the thermal response.

At higher latitudes, the cooling produced by a decrease in net radiation can result in an increase in the extent of snow cover and sea ice. The greater area covered by the highly reflective snow and ice results in a further decrease in net radiation, leading to additional cooling. This positive feedback mechanism involving snow cover and sea ice acts to amplify the thermal response at high latitudes.

In addition, at a high latitude location the thermal stratification of the atmosphere is quite stable. Thus in order to compensate for a high latitude decrease in net radiation at the top of the atmosphere a relatively large reduction in temperature is necessary, since the cooling is confined to a relatively shallow layer. This contrasts with the situation at low latitudes where the atmosphere is less stable. There, only a small cooling would be required to offset the change in net radiation, since convection mixes that cooling throughout the troposphere. Since the LGM ice sheets were located primarily north of 50N, the temperature change they induce is larger relative to the radiative forcing than that associated with the changes in land albedo, which occur throughout the continental areas at all latitudes.

In the case of reduced CO_2 the reason for the larger response is somewhat different. Its associated radiative forcing is global in extent, although larger in low latitudes. Unlike the changes in continental ice and land albedo, which produce local changes in the radiation balance only over land, the radiative forcing produced by lower atmospheric CO_2 is effective over both land and sea. The presence of oceanic forcing allows a powerful feedback mechanism to take effect, in which reduced temperatures result in thicker and more extensive sea ice. This increase in sea ice insulates the atmosphere from the relatively warm underlying sea water, allowing air temperature to decrease further. This insulation effect increases the thermal response to the initial radiative forcing. In the case of changes in land albedo the radiative forcing is confined to the continents.

The latitudinal distributions of the differences in annually-averaged zonal mean surface air temperature resulting from expanded continental ice, reduced CO_2, and changes in surface albedo are presented in Fig. 4. The change in temperature produced by incorporating all three is also plotted for comparison. As in the computation of the area averages, only gridpoints that are ice-free in all four experiments are used to calculate the zonal means. As noted previously with regard to the changes in SST, there is a pronounced asymmetry in the response to the ice sheet effect. A dramatic reduction of temperature occurs over much of the Northern Hemisphere, exceeding 5 °C poleward of 50N. Comparison with the total simulated LGM cooling indicates that the ice sheet-induced cooling is responsible for the bulk of the LGM temperature change north of 30N. In contrast, little cooling occurs in the
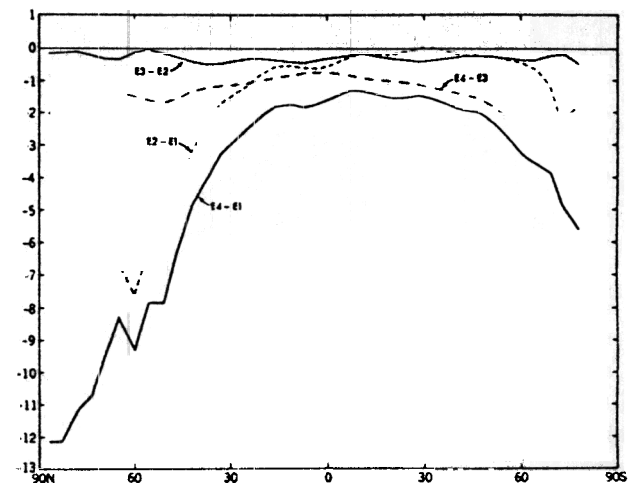

Fig. 4. Latitudinal distribution of annually averaged difference in zonal mean surface air temperature (°C) between the following pairs of experiments: E2-E1 (ice sheet effect), E4-E3 (CO_2 effect), E3-E2 (albedo effect), and E4-E1 (combined effect). Only gridpoints free of continental ice in all four experiments are used in computing the difference

Southern Hemisphere except for the region surrounding Antarctica south of 60S, where thicker and more extensive Antarctic continental ice induces cooling over the nearby oceans. A closer comparison with the zonal mean SST changes in Fig. 3 reveals that the maximum cooling in the Northern Hemisphere is more widespread and extends further north in the case of surface air temperature. The small reduction in SST in the high latitude Northern Hemisphere results from the presence of sea ice, which limits the reduction of SST as discussed in Sect. 4. No such limitation is imposed on the reduction of surface air temperature.

The response of surface air temperature to reduced CO_2 features cooling maxima in the high latitudes of both hemispheres with a minimum of cooling in the tropics. There is little hemispheric asymmetry to the response, with only a slightly greater reduction of temperature in the Southern Hemisphere. A more pronounced tendency for larger Southern Hemisphere cooling is noted in the case of SST, where sea ice limits the Northern Hemisphere response. The decrease in temperature due to the reduction of atmospheric CO_2 is responsible for almost all of simulated LGM Southern Hemisphere cooling. Changes in surface albedo produce a relatively small reduction of surface air temperature, generally less than 0.5 °C at all latitudes. No strong dependence on latitude is obvious for this effect.

Only a limited amount of information about the thermal response of the model to changes in boundary conditions can be extracted from the data presented in Table 4 and Fig. 4. Since the time- and area-averaging used to produce these data may conceal many interesting features of the model's response, the seasonal and geographical distributions of surface air temperature will be examined for each pair of experiments in the following subsections.

5.1. Ice sheets

To examine the changes in surface air temperature resulting from incorporating the LGM distribution of continental ice into the model, experiments E2 and E1 will be compared. Figure 5 maps the difference in annual mean surface air temperature between these two experiments. Most prominent are the centers of large temperature reduction, reaching 20 °C in magnitude, located over the North American and Eurasian ice sheets. This local cooling over the expanded continental ice is not unexpected, since the high albedo of the ice alters the radiation balance and the ice surface attains elevations in excess of 2 km over much of its area. Another region of large cooling is the North Atlantic Ocean, where temperatures are more than 15 °C cooler in the vicinity of the Labrador Sea. Manabe and Broccoli (1985a) discussed the mechanism for this large oceanic cooling, in which air is cooled as it traverses the northern periphery of the North American ice sheet, then flows across the western North Atlantic producing an in-
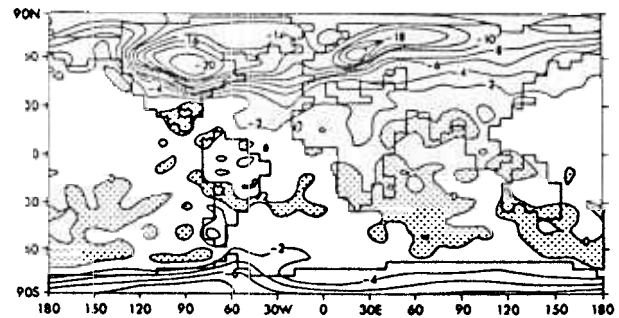

Fig. 5. Difference in annual mean surface air temperature (°C) between experiments E2 and E1, indicative of the response to changes in the ice sheet distribution. Regions of temperature increase are *stippled*

crease in the extent and thickness of sea ice. The resulting thermal insulation of the atmosphere from the underlying sea water produces a large reduction in surface air temperature. The large cooling over the North Atlantic adjacent to the North American and Eurasian ice sheets contributes prominently to the location of the maximum zonally averaged cooling in the high latitude Northern Hemisphere as depicted in Fig. 4.

Another notable feature is the absence of substantial Southern Hemisphere cooling. Many areas in that hemisphere are slightly warmer in E2 as compared with E1, and most others cool only slightly. Exceptions occur over extreme southern South America, where the Patagonian Ice Cap exerts some influence, and over Antarctica, where continental ice is thicker and slightly more extensive in experiment E2. There is some suggestion that the small tropical response may be amplified over continental areas as illustrated by small areas of 2 °C cooling in South America.

In order to examine some of the seasonal variations of the ice sheet effect on temperature, Fig. 6 is constructed. It contains differences in zonal mean surface air temperature
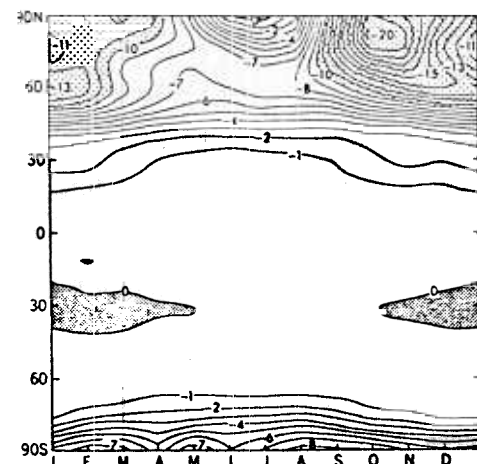

Fig. 6. Latitude-time distribution of the difference in zonal mean surface air temperature (° C) between experiments E2 and E1. *Dense stippling* indicates an increase in temperature, and *light stippling* indicates a temperature decrease of 10 ° C or more

between E2 and E1 plotted as a function of latitude and season. This plot once again shows the hemispheric asymmetry of the response to continental ice. Only the extreme high latitudes of the Southern Hemisphere, where the Antarctic ice sheet is thicker and more extensive, cool as substantially as does the extratropical Northern Hemisphere. Much of the cooling at these latitudes can be attributed to the increased surface elevation, since ice-covered regions are included in this analysis. In all seasons but summer there is a tendency for the temperature difference to increase with increasing latitude in the Northern Hemisphere; during summer the maximum temperature decrease occurs between 60–70N. An autumn maximum of cooling develops at 80N and extends equatorward to 60N by midwinter. An analogous feature of opposite sign was found in the CO_2-quadrupling experiment of Manabe and Stouffer (1980), who attributed it to decreases in sea ice thickness and consequent reduction of heat conduction through the ice. An increase of ice thickness is responsible for the feature found in this study.

From 20–50N, equatorward of the majority of continental ice, the ice sheet-induced cooling is largest in winter and smallest in summer. The primary reason for this seasonal variation is the change in the influence of thermal advection on surface air temperature. In winter, air cooled over the ice sheets is advected across nearby ice-free regions, thereby reducing the temperature. During summer, when winds are weaker and solar radiation stronger, thermal advection is not as large an influence on surface air temperature. In addition, the snow-albedo-temperature feedback process over the continents operates more strongly during the cold season, as discussed by Manabe and Broccoli (1985a). A similar but much weaker winter maximum of midlatitude cooling can be found in the Southern Hemisphere.

5.2. Reduced CO_2

The model's sensitivity to the reduction of atmospheric CO_2 content from modern levels to those estimated for the LGM (Neftel et al. 1982) can be examined by contrasting experiments E4 and E3. To examine the geographical distribution of the changes in annual mean surface air temperature associated with reduced CO_2, Fig. 7 is constructed. A prominent characteristic of the CO_2 effect is the relatively small cooling found in the tropics, where the reduction in temperature is generally less than 1 °C. This contrasts with a larger cooling in the high latitude regions of both hemispheres. As mentioned previously, this polar amplification of the temperature response resulting from reduced atmospheric CO_2 has also been found in model studies of CO_2 increase. It is attributable to feedbacks involving snow and sea ice and to the greater static stability of the high latitude atmosphere, which produces large temperature changes in a relatively shallow surface layer as
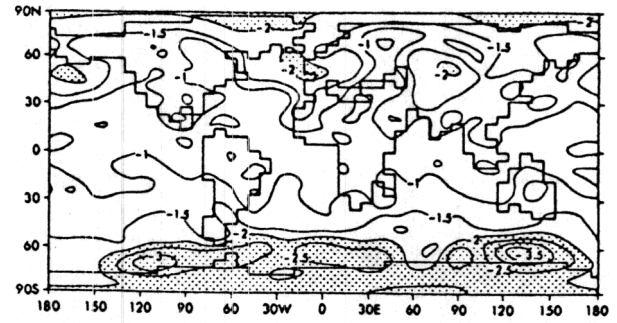

Fig. 7. Difference in annual mean surface air temperature (° C) between experiments E4 and E3, indicative of the response to reduced CO_2. Stippling indicates regions in which the temperature decrease is greater than 2 °C

discussed previously. Also prominent is the belt of large surface air temperature decrease surrounding Antarctica. This is associated with an expansion of Southern Hemisphere sea ice and the resulting albedo feedback and insulation of the atmosphere from the underlying water. Less pronounced cooling maxima are also found over regions of expanded sea ice in the North Atlantic and North Pacific oceans.

Other notable features are relative maxima of cooling located over central Asia (near 90E) and southeastern North America. Analysis of changes in the computed surface albedo suggests that these maxima are associated with regions of increased snow-albedo-temperature feedback produced by increases in the extent, frequency, and thickness of snow cover. Local minima of temperature reduction are located over the Eurasian and North American ice sheets. These can be associated with the absence of snow-temperature-albedo feedback, since these ice sheets are covered with thick snow all year long in both experiments.

A latitude-time plot of the difference in zonal mean surface air temperature (Fig. 8) between experiments E4 and E3 allows some evaluation of the seasonal response. This plot shows clearly that the polar amplification of the thermal response is primarily a cold season phenomenon, with the largest cooling at high latitudes occurring primarily during late autumn and winter in each hemisphere. As a corollary, seasonal variation of the temperature reduction occurs primarily at high latitudes.

A late autumn cooling maximum, similar to that produced by the ice sheet effect and analogous to a maximum of warming found in some studies of CO_2 increase (Manabe and Stouffer 1980), is weakly present in the response to reduced CO_2. An examination of differences in sea ice thickness, ocean albedo, and the vertical thermal gradient across the sea ice suggests that feedbacks involving the albedo and thermal conductivity of sea ice are responsible for this maximum, as discussed by Manabe and Stouffer (1980). The greater sea ice area in both experiments E4 and E3 shifts the late autumn-early winter
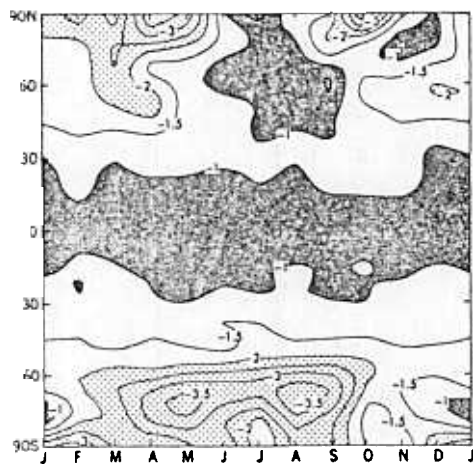
Fig. 8. Latitude-time distribution of the difference in zonal mean surface air temperature (° C) between experiments E4 and E3. *Dense stippling* indicates a decrease in temperature smaller than 1 °C, and *light stippling* indicates a temperature decrease greater than 2 °C

temperature reduction maximum to a lower latitude. This is manifested in the weak maximum of cooling just south of 60N from October through January. The relatively high land fraction at these latitudes reduces the impact from this mechanism on the zonally averaged cooling.

5.3. Land albedo

By comparing experiments E3 and E2, the model's sensitivity to the LGM changes in land surface albedo can be studied. It is important to note that the changes prescribed include only those resulting from changes in prevailing vegetation and soil type as reconstructed by CLIMAP; the LGM ice sheets are used in both experiments. The difference in annual mean surface air temperature is mapped in Fig. 9. In contrast to the effects of the expanded ice sheets and reduced CO_2, the albedo effect is smaller and more regional in nature. The magnitude of these changes tends to be small compared to the model's interannual variability, so that most of the regions of temperature change fail tests
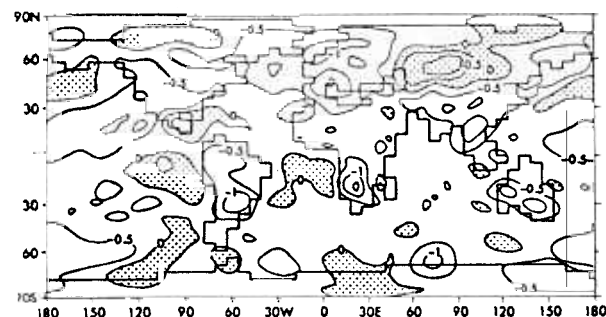

Fig. 9. Difference in annual mean surface air temperature (°C) between experiments E3 and E2, indicative of the response to changes in land albedo. Regions of temperature increase are *stippled*

for statistical significance at the 10% level (Chervin and Schneider 1976). Exceptions over land are the areas of reduced temperature in southern Africa, southeast Asia, southern Australia, and much of South America. Over the oceans, the very modest cooling of the subtropical North Pacific and the Mediterranean Sea region is significant due to the small interannual temperature variations over water.

Some association can be made between these areas and the land albedo changes themselves, which are mapped in Fig. 2. Ice age albedo increases occurred in all but the heavily stippled areas, in which albedos were lower at the LGM. Thus the net globally-averaged cooling of 0.3 °C associated with the LGM land albedos is consistent with the widespread increases in albedo. Areas of substantial albedo increase are present corresponding to many of the areas of cooling, such as those over South America, southern Australia, and the Medierranean. Other regions of increased albedo located at higher latitudes, including some Northern Hemisphere areas with albedo increases of more than 5%, are not associated with significant temperature changes since snow cover frequently masks the surface in these areas. The albedo effect on temperature appears to be most important over low latitude continents where insolation is large and there is no masking by snow cover.

6. Response of atmospheric circulation

It has been assumed that the pronounced changes in temperature that characterized glacial times were accompanied by significant changes in atmospheric circulation. Lamb and Woodroffe (1970) used paleoclimatic estimates of surface temperature to derive hypothetical flow patterns for the 500 mb level and the surface. In ice age simulation studies using GCMs, Williams et al. (1974), Gates (1976b), and Kutzbach and Guetter (1986) examined the model-generated tropospheric circulation, comparing it with the simulated modern circulation. In each of these studies, substantial differences were noted between the ice age and modern cases. Manabe and Broccoli (1985a) also found large changes in mid-tropospheric circulation between GCM runs with and without the continental ice sheets of the LGM.

To examine the changes in circulation associated with the current model's simulation of the LGM climate and how continental ice, reduced CO_2, and changes in land albedo contribute to these changes, Fig. 10 is constructed. It depicts the Northern Hemisphere winter circulation at the 500 mb level for experiments E1, E2, and E4. In comparing the simulations of the modern and LGM circulation (experiments E1 and E4), most notable is the high amplitude ridge-trough pattern over the North American continent and North Atlantic Ocean in the LGM case. This represents an amplification of the weak ridge-trough pattern that occurs in the modern simulation.
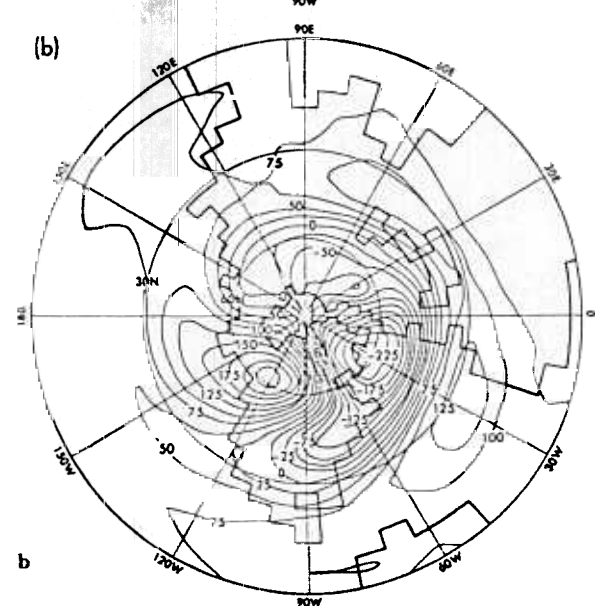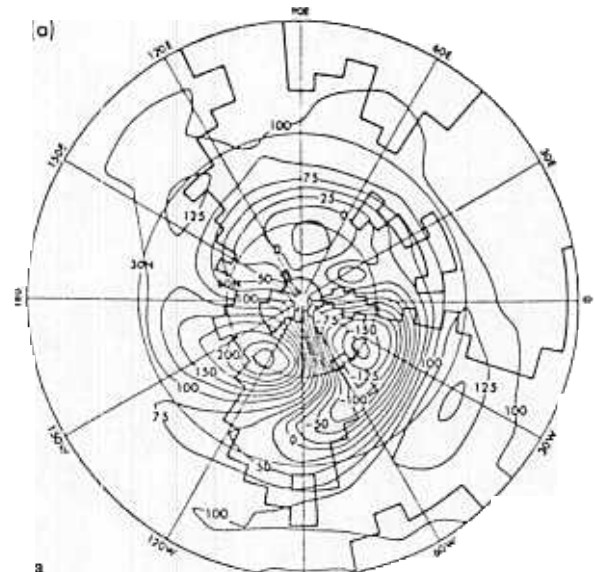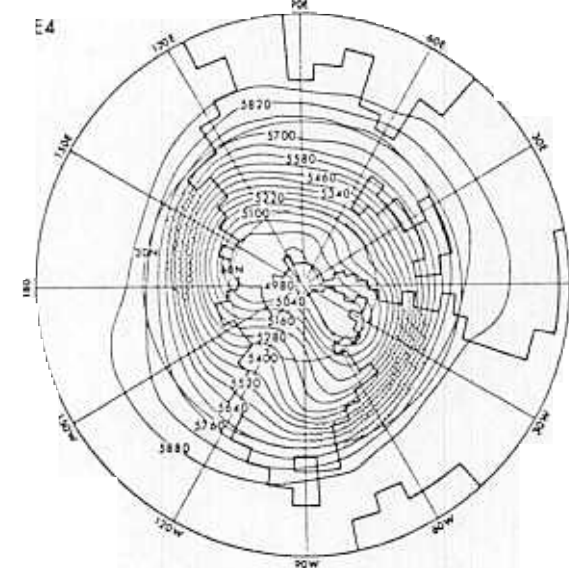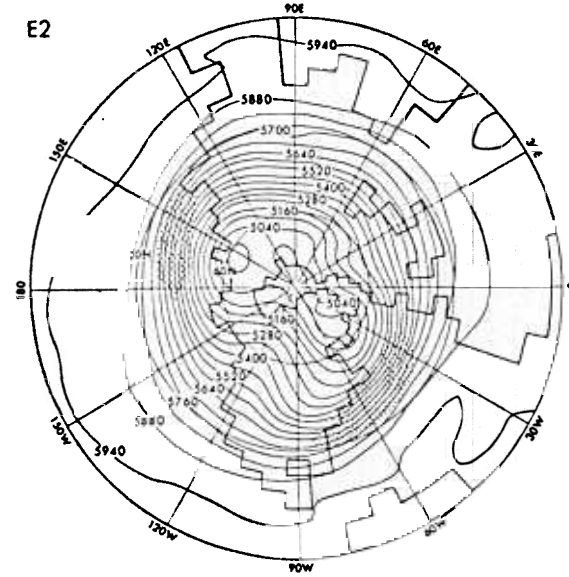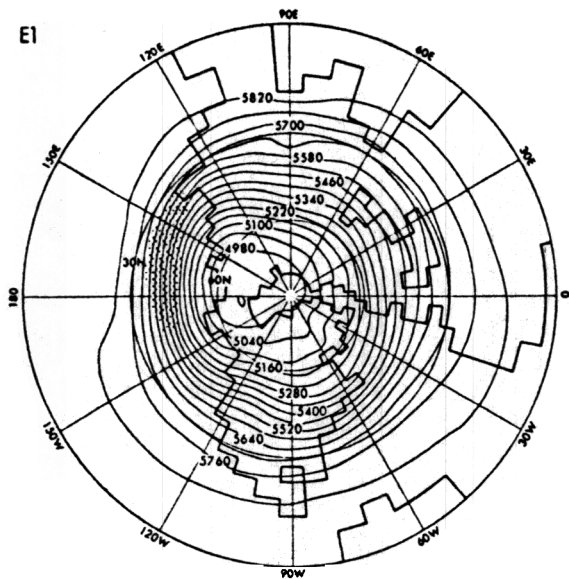
E1

E2

E4

(a)

(b)

Fig. 11a and b. Northern Hemisphere distribution of difference in 500 mb geopotential height (m) during winter (December-January-February) between a experiments E2 and E1 and b experiments E4 and E1

To aid in identifying the changes in 500 mb flow, maps of the differences in geopotential height between experiments E4 and E1 and experiments E2 and E1 are presented in Fig. 11. An enhancement of the northerly component of the flow can be noted over the eastern portion of the Canadian arctic islands as a result of the enhanced ridge over western North America and the deepened trough over Greenland and the North Atlantic. Increased southerly flow occurs to the west of the North American ridge into the

◄ Fig. 10. Northern Hemisphere distribution of 500 mb geopotential height (m) during winter (December-January-February) for experiments E1, E2, and E4. *Stippling* indicates wind speeds greater than 30 m s⁻¹
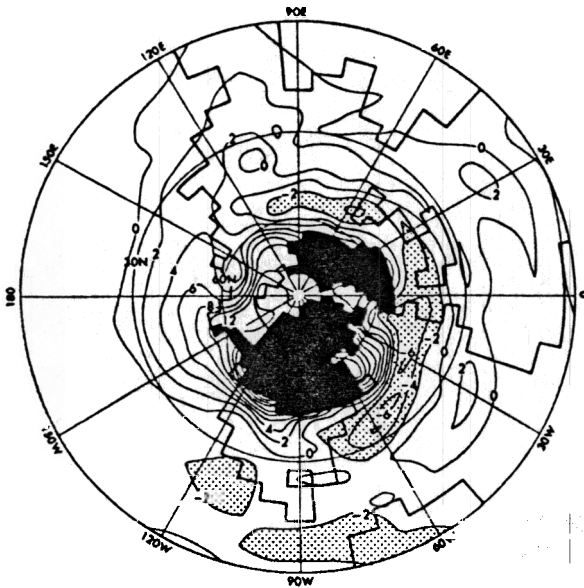
Fig. 12. Difference in Northern Hemisphere sea level pressure (mb) between experiments E4 and E1 during winter (December-January-February). A uniform value of 16 mb has been subtracted in order to eliminate the ice sheet-induced change in global mean sea level pressure. The areas of elevated ice sheet topography have been blacked out, and *stippling* indicates decreases of sea level pressure greater than 2 mb

Fig. 13. Difference in Northern Hemisphere winter (December-January-February) precipitation (cm d^{-1}) between experiments E4 and E1. Regions of increased precipitation are *stippled*

Alaskan region. In addition, the middle latitude westerlies are strengthened substantially from eastern North America across southern Europe and into central Asia. This is evident from the appearance of the 30 m s^{-1} isotach over the North Atlantic in Fig. 10, and the anomalous westerly flow implied in Fig. 11b. A belt of reduced sea level pressure (Fig. 12) parallels the region of enhanced westerlies from the western North Atlantic into central Asia. Increased storminess is also found along the axis of this belt. To the south, a strengthening of the subtropical ridge occurs from the eastern Atlantic across northern Africa and the Arabian peninsula.

Features similar to some of these have been noted in other GCM simulations of the ice age climate. Williams et al. (1974) found a band of increased cyclonic activity extending from the western North Atlantic eastward to the southern edge of the Scandinavian ice sheet and into central Asia. In the studies by Manabe and Broccoli (1985a) and Kutzbach and Guetter (1986), enhanced westerlies were found across the North Atlantic into Europe, as was the amplified ridge-trough pattern over North America.

Comparing the results from experiments E2 and E4 (Figs 11a and 11b), most of the changes in 500 mb circulation present in the LGM simulation (E4) are apparent when continental ice alone is incorporated in the model (E2). However, the lowering of heights in the North Atlantic is not quite as pronounced in E2 as in E4, nor is the enhancement of the westerly flow across the Eurasian continent. The additional prominence of these features in the LGM
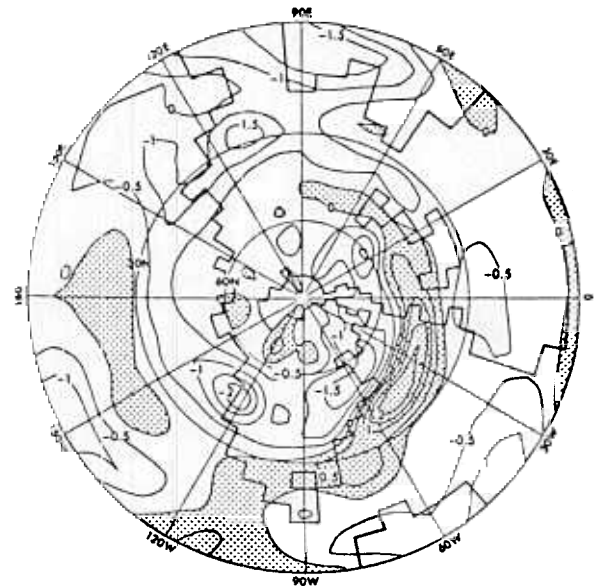
simulation appears to be associated with the effects of reduced CO_2, since the addition of land albedo changes produces little difference in circulation between experiments E2 and E3 (not shown).

Some of these changes in circulation may have interesting implications for the growth and maintenance of the Northern Hemisphere ice sheets. The enhanced northerly flow over eastern sections of the Laurentide ice would be likely to aid in cooling its southeastern margin, where the ice attains its lowest latitude. Additionally, the storm track associated with the strengthening of the westerlies from the western Atlantic across much of Eurasia skirts the southeastern corner of the Laurentide ice and the entire southern edge of the Scandinavian ice sheet. Increased precipitation is associated with this belt of storminess, as indicated in Fig. 13, which shows the differences in Northern Hemisphere winter precipitation between experiments E4 and E1. This precipitation, which falls primarily in the form of snow, is important to the snow budgets of these ice sheets. Since these changes in circulation occur in the experiment with expanded continental ice alone, the possibility is raised of a self-sustaining mechanism for ice sheet growth and maintenance. To evaluate the importance of this mechanism to ice sheet growth would require experiments in which the climatic effect of smaller ice sheets, representative of the early stages of glaciation, is examined.

7. Concluding remarks

This study investigates the contributions of expanded continental ice, reduced atmospheric CO_2, and changes in

land albedo to the maintenance of the LGM climate. In an earlier study, Manabe and Broccoli (1985b) found that incorporating all three of these factors produced a thermal response of comparable magnitude to paleoclimatic data from the LGM. In the current study, both the ice sheet and CO_2 effects are found to be required in order to produce sufficient cooling on a global basis. The expansion of continental ice produces much of the Northern Hemisphere cooling, but has only a very minor influence on Southern Hemisphere temperature. This result is consistent with a previous study of the effects of continental ice on climate (Manabe and Broccoli 1985a). In that study, the loss of heat energy due to the reflection of solar radiation by Northern Hemisphere continental ice is almost entirely compensated by a reduction in the upward terrestrial radiation from that hemisphere. As a result, little change in interhemispheric heat transport occurs despite the cooling of the Northern Hemisphere, so there is little change in Southern Hemisphere temperature.

Most of the cooling in the Southern Hemisphere results from the reduction of CO_2. Changes in land albedo over ice-free regions have only a small effect on global temperature, although they have a substantial local influence in some low latitude locations. The thermal effects of both expanded continental ice and reduced CO_2 show a polar amplification and a late autumn-early winter maximum similar to those found in earlier studies of CO_2 increase. The amount of cooling resulting from each of the changes in boundary conditions is roughly consistent with the radiative forcing associated with each change.

The role of reduced CO_2 in maintaining an ice age climate is particularly interesting given the difficulties in reconciling the approximate simultaneity of glacial periods in both hemispheres with the Milankovitch forcing of Pleistocene climate fluctuations. Mechanisms have been proposed by which Northern Hemisphere glaciation would trigger a reduction in atmospheric CO_2 (see, for example, Broecker 1984). Such a mechanism may represent a way in which a Northern Hemisphere climatic signal could be transmitted into the Southern Hemisphere. The results from this study confirm the finding of Manabe and Broccoli (1985a) that the introduction of expanded continental ice into the model does little to cool the Southern Hemisphere. In addition, a reduction of atmospheric CO_2 to the levels estimated for the LGM produces substantial Southern Hemisphere cooling. This supports the hypothesis that glacial-interglacial variations in CO_2 concentration may provide a linkage between the two hemispheres. The experiments performed in this study do not address the possibility that changes in ocean circulation during glacial times may be responsible for cooling the Southern Hemisphere, since the model used does not include an oceanic GCM. Further development of models of the coupled atmosphere-ocean system (e. g., Manabe et al.

1979) is required so that experiments can be performed to evaluate this effect properly.

Boundary conditions from the LGM are found to substantially modify the tropospheric circulation, particularly in the Northern Hemisphere during winter. An amplified ridge-trough pattern at the 500 mb level over North America and the nearby North Atlantic Ocean is associated with anomalous northerly flow over the eastern portions of the Laurentide ice dome. The middle latitude westerlies are strengthened from the western Atlantic across much of Eurasia. These enhanced westerlies are accompanied by a belt of reduced sea level pressure and increased storminess. In examining the effects of each of the changes in boundary conditions individually, these alterations in tropospheric circulation result primarily from the ice sheet effect.

References

Berlyand TG, Strokina LA, Greshnikova LE (1980) Zonal cloud distribution on the earth. Meteorol Gidrol 3: 15-23

Bourke W (1974) A multi-level spectral model I. Formulation and hemispheric integrations. Mon Weather Rev 102: 687-701

Broecker WS (1984) Carbon dioxide circulation through ocean and atmosphere. Nature 308: 602

Chervin RM, Schneider SH (1976) On determining the statistical significance of climate experiments with general circulation models. J Atmos Sci 33: 405-412

CLIMAP Project Members (1976) The surface of the ice-age earth. Science 191: 1131-1137

CLIMAP Project Members (1981) Seasonal reconstructions of the earth's surface at the last glacial maximum. Geol Soc Am Map Chart Ser, MC-36

Gates WL (1976a) Modeling the ice-age climate. Science 191: 1138-1144

Gates WL (1976b) The numerical simulation of ice-age climate with a global general circulation model. J Atmos Sci 33: 1844-1873

Gordon CT, Stern WF (1982) A description of the GFDL global spectral model. Mon Weather Rev 110: 625-644

Hansen J, Lacis A, Rind D, Russell G, Stone P, Fung I, Ruedy R, Lerner J (1984) Climate sensitivity: analysis of feedback mechanisms. In: Hansen J, Takahashi T, (eds) Climate processes and climate sensitivity. Maurice Ewing Series, 5, pp 130-163

Hays JD, Imbrie J, Shackleton NJ (1976) Variations in the earth's orbit: pacemaker of the ice age. Science 194: 1121-1132

Kutzbach JE, Guetter PJ (1986) The influence of changing orbital parameters and surface boundary conditions on climate simulations for the past 18 000 years. J Atmos Sci 43: 1726-1759

Lamb HH, Woodroffe A (1970) Atmospheric circulation during the last ice age. Quat Res 1: 29-58

London J (1957) A study of atmospheric heat balance, final report. Contract AF19(122)-165 DDC, Coll of Engl, New York University, (NTIS AD 117227)

Manabe S, Broccoli AJ (1985a) The influence of continental ice sheets on the climate of an ice age. J Geophys Res 90: 2167-2190

Manabe S, Broccoli AJ (1985b) A comparison of climate model sensitivitiy with data from the last glacial maximum. J Atmos Sci 42: 2643-2651

Manabe S, Bryan K, Spelman MJ (1979) A global ocean-atmosphere climate model with seasonal variation for future studies of climate sensitivity. Dyn Atmos Ocean 3: 393-426

Manabe S, Hahn DG (1977) Simulation of the tropical climate of an ice age. J Geophys Res 82: 3889-3911

Manabe S, Stouffer RJ (1980) Sensitivity of a global climate model to an increase of CO_2 concentration in the atmosphere. J Geophys Res 85: 5529-5554

Milankovitch M (1941) K Serb Akad Beogr Spec Publ 132, translated from German by the Israel Program for Scientific Translations, Jerusalem

Neftel A, Oeschger H, Schwander J, Stauffer B, Zumbrunn R (1982) Ice core sample measurements give atmospheric CO_2 content during the past 40 000 yr. Nature 295: 200-223

Shackleton NJ, Hall MA, Line J, Shuxi C (1983) Carbon isotope data in core V19-30 confirm reduced carbon dioxide concentration in the ice age atmosphere. Nature 306: 319-322

Williams J, Barry RG, Washington WM (1974) Simulation of the atmospheric circulation using the NCAR global circulation model with ice age boundary conditions. J Appl Meteorol 13: 305-317